

JGR Space Physics

RESEARCH ARTICLE

10.1029/2018JA026049

D-Region High-Latitude Forcing Factors

Edith L. Macotela¹ , Mark Clilverd² , Jyrki Manninen¹ , Tracy Moffat-Griffin² , David A. Newnham² , Tero Raita¹ , and Craig J. Rodger³ 

¹Sodankylä Geophysical Observatory, University of Oulu, Sodankylä, Finland, ²British Antarctic Survey (UKRI), Cambridge, UK, ³Department of Physics, University of Otago, Dunedin, New Zealand

Key Points:

- D-region periodic variations are studied using wavelet analysis of 10 years of high-latitude subionospheric VLF waves
- Mesospheric temperature is more related to daytime VLF annual oscillations but nighttime is more related to solar Lyman- α flux
- The 27-day solar rotation period dominates solar declining phase and all periods shorter than annual are transitory

Correspondence to:

E. L. Macotela,
edith.macotelacruz@oulu.fi

Citation:

Macotela, E. L., Clilverd, M., Manninen, J., Moffat-Griffin, T., Newnham, D. A., Raita, T., & Rodger, C. J. (2019). D-region high-latitude forcing factors. *Journal of Geophysical Research: Space Physics*, 124, 765–781. <https://doi.org/10.1029/2018JA026049>

Received 30 AUG 2018

Accepted 22 DEC 2018

Accepted article online 12 JAN 2019

Published online 30 JAN 2019

Abstract The subionospheric very low frequency (VLF) radio wave technique provides the possibility of investigating the response of the ionospheric D-region to a diversity of transient and long-term physical phenomena originating from above (e.g., energetic particle precipitation) and from below (e.g., atmospheric waves). In this study, we identify the periodicities that appear in VLF measurements and investigate how they may be related to changes in space weather and atmospheric activity. The powerful VLF signal transmitted from NAA (24 kHz) on the east coast of the United States, and received at Sodankylä, Finland, was analyzed. Wavelet transform, wavelet power spectrum, wavelet coherence, and cross-wavelet spectrum were computed for daily averages of selected ionospheric, space weather, and atmospheric parameters from November 2008 until June 2018. Our results show that the significant VLF periods that appear during solar cycle 24 are the annual oscillation, semiannual oscillation, 121-day, 86-day, 61-day, and solar rotation oscillations. We found that the annual oscillation corresponds to variability in mesospheric temperature and solar Lyman- α (Ly- α) flux and the semiannual oscillation to variability in space weather-related parameters. The solar rotation oscillation observed in the VLF variability is mainly related to the Ly- α flux variation at solar maximum and to geomagnetic activity variation during the declining phase of the solar cycle. Our results are important since they strengthen our understanding of the Earth's D-region response to solar and atmospheric forcing.

1. Introduction

Very low frequency (VLF: 3–30 kHz) radio signals propagate inside the Earth-ionosphere waveguide and can be used to monitor the electrical conductivity of the waveguide's upper boundary (Wait & Spies, 1964). This upper boundary fluctuates in the altitude range ~60–90 km from day to night and is known as the D-region (Hargreaves, 1992; Samanes et al., 2018). The lower ionosphere can be affected by sporadic (Bracewell & Straker, 1949) or periodic (McWilliams & Strait, 1976) external forces. As a result, they can be detected using subionospheric VLF wave analysis techniques.

Periodic variations of solar (Demirkol et al., 1999; Thomson & Clilverd, 2000) and terrestrial (Samanes et al., 2018) origin affect recorded VLF signals over long- or short-time scales. Many studies show long-term periodic variations of solar origin, such as the 11-year solar cycle, in the lower ionosphere (e.g., Macotela et al., 2017; Thomson & Clilverd, 2000). However, limited studies have been done using VLF data recorded at high-latitude regions, where long-term geomagnetic activity might be expected to strongly influence the VLF signals (e.g., Clilverd et al., 2010). There are also only a few reports on short-term solar variations, that is, associated with the 27-day solar rotation, in the lower ionosphere (Demirkol et al., 1999; McWilliams & Strait, 1976). These studies used nighttime VLF data recorded at high-latitude and midlatitude regions to show solar related short-term variations. However, no formal analysis of the frequency content of the VLF signal variations was made. Therefore, it is necessary to undertake a more detailed identification of periodicities in the VLF signals in order to uncover their possible sources.

Previous studies have reported the influence of the annual oscillation (AO) and semiannual oscillation (SAO) using ground-based VLF narrowband measurements (Samanes et al., 2018; Sharma et al., 2017; Silber et al., 2016). Silber et al. (2016) applied the Lomb-Scargle method to recorded VLF signals that had propagated in low-latitude and midlatitude regions, to determine the dominant oscillations in the nighttime VLF measurements. They showed that the most dominant periodicities were ~343 and ~180 days. The authors suggested that the SAO modulation in VLF measurements were due to nitrogen oxides (NO_x) transport. Another significant oscillation reported by Silber et al. (2016) was a periodicity of 241 days (~8 months).

However, no mechanism was suggested for this unexpected oscillation period. Sharma et al. (2017) used daytime and nighttime recorded VLF signals that propagated in midlatitude regions to detect the AO and SAO oscillations. They applied the same method described by Silber et al. (2016) and found that VLF measurements exhibit more oscillations besides the SAO and AO. No explanation was suggested by the authors for those additional oscillations. However, the findings of Sharma et al. (2017) did agree with Silber et al. (2016) that the SAO is the strongest oscillation detected in midlatitude nighttime VLF measurements. Using the Lomb-Scargle method, periodicities related to the AO, SAO, and quasi biennial oscillation were reported by Samanes et al. (2018). They analyzed the derived nighttime reflection height using signals that propagated in low-latitude regions. Besides the studies of AO and SAO, Pal et al. (2015) reported that the nighttime VLF amplitude signal also contained a 27-day periodicity. They applied fast Fourier transform analysis to VLF signals that propagated in midlatitude and low-latitude regions. The authors suggested that the 27-day period could be related to the 27-day variability of solar irradiance.

From previous studies it is clear that different approaches have been used to show the variability of the lower ionosphere to periodic variations of solar or atmospheric origin. The midlatitude daytime VLF data show the 11-year solar cycle, AO, and SAO, while the nighttime VLF data show the AO, SAO, and also indications of periods related to solar rotation oscillation. However, there is a lack of understanding of possible sources of induced oscillations observed in VLF measurements and few studies have included high-latitude paths where geomagnetic activity influence is important. Thus, in this study we apply the wavelet technique to analyze VLF data recorded in high-latitude regions in order to identify the oscillations contained in the signal and the possible sources of those oscillations. Wavelet analysis is a tool for analyzing nonstationary variations of power within a time series (Torrence & Compo, 1998). However, until now this useful technique has been mainly applied to geophysical studies such as seismology and neutral atmosphere dynamics (Van den Berg, 1999). Furthermore, there are very few reports on the analysis of VLF signals using the wavelet technique (e.g., Kumar et al., 2017; Maurya et al., 2014). Due to the capacity of wavelet analysis of determining how the dominant modes of a time series vary with time, there are potential applications of the wavelet technique to space weather studies (Aguilar-Rodriguez et al., 2014). This technique has huge advantages compared with the Lomb-Scargle and fast Fourier transform methods, which do not describe any the temporal variation of signals contained in a time series.

The aim of the present study is to examine daytime and nighttime VLF amplitude oscillations, on a high-latitude subionospheric VLF propagation path, that are caused by space weather and atmospheric activity during solar cycle 24, that is, data from 2008–2018. By decomposing the VLF time series into the time-frequency domain, we determine both the dominant modes of variability and how those modes vary with time. By employing the wavelet coherence (WTC) and cross-wavelet transform (XWT) we examine the relationship in the time-frequency domain between the VLF and space weather and atmospheric time series. In this way, we look for possible sources of the oscillations found in the VLF data, which is an improvement with respect to previous analysis. We outline how combining the VLF remote sensing technique with wavelet analysis can be developed to investigate factors that influence the behavior of the lower ionosphere. In section 2 the data used in this work and the methodology applied for the analyses are presented. The results obtained are given in section 3. The interpretation of the results and summary of the study are in section 4.

2. Data and Methods

This section describes the approach used to obtain the daily averages of the ionospheric, space weather, and mesospheric measurements that we employ in the wavelet study. Daily values were computed because periodicities, in the parameters, of less than 1 day are not of interest to this study. A brief explanation why the data sets are used is also included in this section. The section ends with a brief explanation of the wavelet analysis and how the results should be interpreted.

2.1. Subionospheric Data

In this study, the narrow band subionospheric VLF data from the 24 kHz transmitter (call sign NAA, 44.6°N, 67.3°W) located on the east coast of the United States and received at Sodankylä, Finland (SOD, 67.4°N, 26.7°E), were analyzed. SOD is part of the Antarctic-Arctic Radiation-belt (Dynamic) Deposition-VLF Atmospheric Research Konsortium (AARDDVARK) network (Ciliverd et al., 2009). The SOD receiver

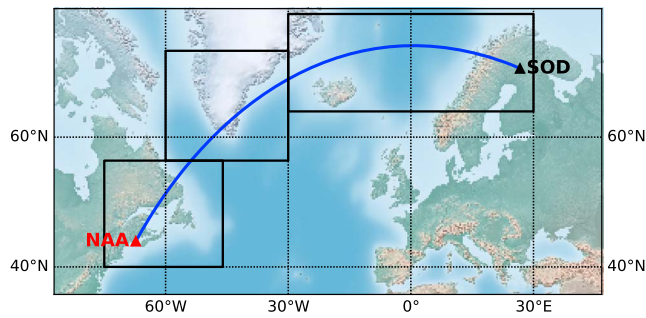


Figure 1. Map showing the location of the transmitter (NAA), the receiver (SOD), and the very low frequency propagation path monitored (blue line). The thick boxes spot areas around the very low frequency propagation path from where the measured atmospheric temperature was used (see section 2.3 for details).

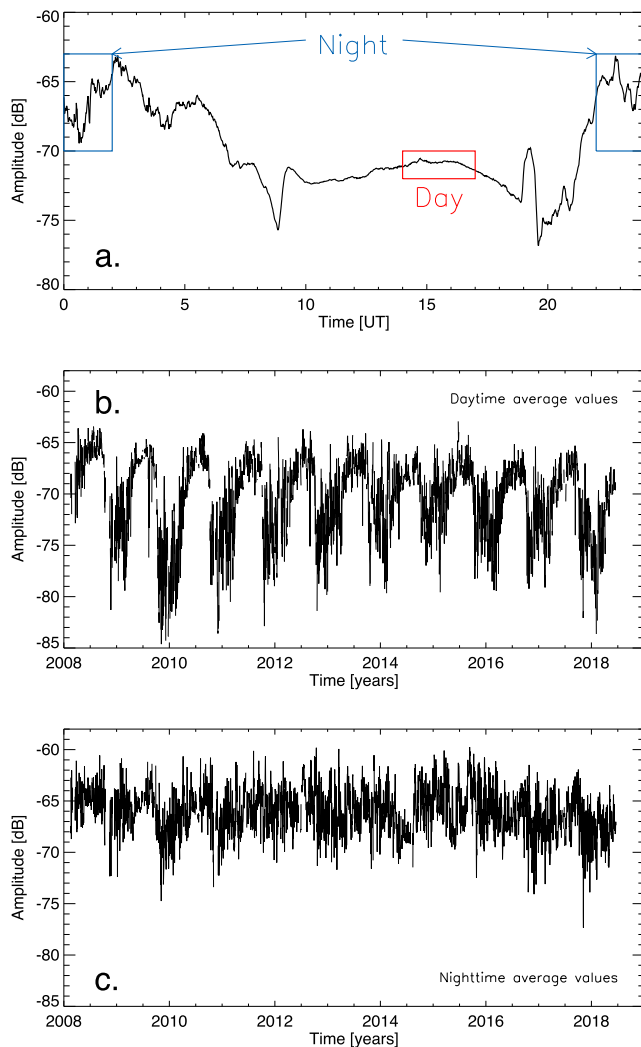


Figure 2. (a) An example of the 24-hr time evolution of the amplitude of the very low frequency signal recorded at Sodankylä on 15 August 2010. Daily average of the daytime (b) and nighttime (c) very low frequency amplitude. Gaps are missing data.

provides continuous long-range observations of the lower ionosphere in the polar regions, and as such we use the VLF data as a proxy for D-region behavior. The receiver software used in Sodankylä is the UltraMSK, which is a package designed to record the phase and amplitude of Minimum Shift Keying modulated narrowband VLF radio signals. Further information about the receiver is available from the URL www.ultramsk.com. The VLF receiver at SOD is composed of two orthogonal loop antennas, one oriented east-west and the other north-south. Magnetic field aeriels are insensitive to environmental factors such as temperature (Watt, 1967). Furthermore, the VLF instrument at SGO is specifically maintained to operate at constant gain. Comparison against a second, independent instrument indicated negligible gain change over 3 years of operation (Neal et al., 2015). Additionally, logged system changes (e.g., wiring repairs) from 2004 onward had no influence on system gain. The stable VLF receiver characteristics make the Sodankylä measurements suitable for monitoring periodicities during solar cycle 24.

The NAA amplitude data sensed by the east-west loop aerial recorded from November 2008 to June 2018 were used in this study. The NAA transmitting signal was chosen because its power is sufficiently constant throughout the collected data set and because there were very few significant data gaps due to transmitter or receiver maintenance. Figure 1 shows the spatial configuration of the transmitter (NAA), the receiver (SOD), and the great circle propagation path between the transmitter and receiver (blue curve). The map shows that the majority of the VLF path is at latitudes poleward of 60°N and can thus be considered as representing high-latitude conditions (Thomson et al., 2018). The thick boxes represent the regions around the VLF propagation path from where atmospheric temperature data were used (see section 2.3 for details) in order to compare against the observations made on the VLF path.

Figure 2 shows the NAA-SOD VLF amplitude data set. The upper panel shows the temporal evolution of VLF amplitude measured at SOD on an example day, that is, 15 August 2010. The amplitude time profile illustrates sunrise and sunset fading transitions over the VLF propagation path observed at 07:00–10:00 and 10:00–20:00 UT, respectively. In this panel the red and blue boxes represent the time windows from 14:00 to 17:00 UT and from 22:00 to 02:00 UT, which were used to compute the average daytime and nighttime daily values, respectively. These times were fixed for all the analyzed years and characterize the noon and midnight conditions over the VLF propagation path. This approach also helps minimize ionospheric short-term fluctuations. The temporal evolution of these daily averages, from 2008 until 2018, is shown in the middle and lower panels of Figure 2 for daytime and nighttime conditions, respectively. Occasional missing data, shown as gaps in Figure 2, was caused by NAA transmitter or SOD receiver maintenance. The period shown covers the extreme solar minimum of 2009, and weak solar maximum in 2014, and the declining phase of the solar cycle from 2015 onward. The NAA transmitter amplitude at SOD is typically 35 dB above the background noise levels, which are mainly due to distant lightning activity.

The full VLF daytime series in Figure 2b exhibits a strong AO. But no other oscillatory behavior can be easily observed by eye. Interestingly, the difference in daytime amplitude between summer and winter is smaller at solar maximum than during the other phases of the solar cycle. In the case of the nighttime VLF time series no dominant oscillation is

clearly exhibited. Thus, in order to determine the important periodicities in the VLF signals, the wavelet technique is applied independently to these two time series, namely, daytime and nighttime. The results of the wavelet analysis are presented in the next section.

2.2. Space Weather Data: Solar and Geomagnetic Activity

Solar Lyman- α (Ly- α) radiation is the main source of ionization of the quiescent lower ionosphere (Nicolet & Aikin, 1960) sensed by the propagation of VLF waves. During daytime direct solar Ly- α radiation creates the D-region, while during nighttime the scattered Ly- α radiation by the geocorona is one of the main sources that maintain the lower ionosphere. Thus, the common periods between Ly- α and the VLF amplitude variations are examined in this study. Solar wind velocity and geomagnetic indices data are also used because changes in the properties of the solar wind produce different responses of the magnetosphere and in this way, variations in geomagnetic activity. Depending on the geomagnetic conditions, precipitating electrons can produce changes in the ionization levels (Thorne & Larsen, 1976) and chemistry (Callis et al., 1991; Turunen et al., 2009) of the lower ionosphere that can affect VLF propagation. Thus, variations associated with geomagnetic activity can also be sensed by VLF wave propagation analysis. Precipitating electrons that affect the lower ionosphere are composed of particles with energies lower than 0.4 MeV, but also of higher fluxes of electrons from 0.4 to 2 MeV (Clilverd et al., 2008). Therefore, electrons in these two energy ranges, that is, <0.4 and >0.4 MeV, are employed in the study to determine their common periodic variations with the VLF amplitude variability.

To examine the induced oscillations in the VLF signal due to solar and geomagnetic activity we use daily values of Ly- α flux, solar wind velocity, the *AE* index, and *Ap* index. These data were obtained from NASA/Goddard Space Flight Center's OMNI data set through the OMNIWeb interface (<https://omniweb.gsfc.nasa.gov/form/dx1.html>). The Ly- α flux and solar wind velocity are measured at fixed distances from the Sun, thus removing any orbital eccentricity factor. Daily average values of electron fluxes at geosynchronous Earth orbit, with energies >0.6 MeV, and energetic electron precipitation (EEP), with energies >30 keV, are also used in this study. Trapped electron fluxes at geosynchronous Earth orbit were provided by the Energetic Particle Sensor instrument on board the Geostationary Operational Environment Satellites (Onsager et al., 1996), while the EEP fluxes were obtained from the Medium Energy Proton and Electron Detector on board the Polar-orbiting Operational Environmental Satellite (Evans & Greer, 2004). The electron fluxes measured by Geostationary Operational Environment Satellites indicate the intensity of the outer electron radiation belt at geostationary orbit. These trapped fluxes are used as a proxy to describe the high-latitude, high-energy, electron precipitation (Clilverd et al., 2008; Simon Wedlund et al., 2014) into the D-region along the NAA-SOD path. The EEP flux data were treated as follows. The fluxes at $L = 3-7$ were averaged, suppressing the measurements in the South Atlantic Magnetic Anomaly region, where inner radiation belt protons swamp the electron detectors (Rodger et al., 2013). Low energy proton contamination corrections were applied using the Lam et al. (2010) algorithm. Finally, periods where solar proton events occurred were removed as the electron data are unlikely to be meaningful at these times.

2.3. Atmospheric Data: Temperature and Nitric Oxide (NO)

Most of the common variability between mesospheric temperatures and daytime VLF amplitude can be explained by global seasonal solar irradiance changes (Silber et al., 2013). However, there are other short-time scale forces affecting daytime VLF signals that are not linked to solar irradiance (Silber et al., 2013). For nighttime VLF signals dynamical processes can be more pronounced (Silber et al., 2016). Silber et al. (2016) suggested that dynamical transport of important species, such as NO molecules, as well as dynamical forces, such as atmospheric waves, are much stronger during nighttime and more easily detected. This suggestion will be examined and also verified in our study.

The Microwave Limb Sounder (MLS) on the Aura satellite observes microwave emissions from a scanning limb view of the atmosphere (Waters et al., 2006). The Aura satellite has a Sun-synchronous near polar orbit at ~700 km altitude with ~13 orbits per day, providing global coverage from 80°N to 82°S, from close to the ground up to approximately 100 km. MLS temperature profiles are retrieved at 54 pressure levels from 261 to 0.001 hPa along each orbital track. The MLS data (version 4, Level 2, ascending nodes), screened using the quality control criteria suggested by Livesey et al. (2017), were used to construct the time series of daily temperature profiles. The regions indicated by the black boxes in Figure 1 are used in order to have enough data samples along the VLF propagation path that will best represent the daily average temperature of NAA-SOD VLF path.

The Solar Occultation For Ice Experiment (SOFIE) instrument (Gordley et al., 2009) on the Aeronomy of Ice in the Mesosphere satellite performs 15 sunrise profile measurements in the Northern Hemisphere, in 16 spectral bands, which are used to retrieve vertical profiles of, among other trace gases, nitric oxide (NO). NO volume mixing ratio (VMR) profiles from 30 to 149 km altitude with height resolution of approximately 2 km are retrieved from observations of the 5.32 μm band. The Northern Hemisphere latitudinal coverage varies throughout the year from 65° to 85°. In this study, we use all the available SOFIE NO data (version 1.3 Level 2, available on sofie.gats-inc.com) measured above 60°N, and between 60°W and 30°E, from November 2008 to March 2015 to obtain the daily vertical NO VMR profiles. The range of data was chosen to overlap available VLF data (since November 2008) and because after March 2015 NO retrievals are limited due to the changes in the Aeronomy of Ice in the Mesosphere orbit (SOFIE data description, http://sofie.gats-inc.com/sofie/SOFIE_Products_V1.3.pdf).

Although MLS and SOFIE both retrieve atmospheric temperature, SOFIE coverage is mainly above 65°N and does not adequately cover the VLF propagation path. MLS coverage offers better opportunities to obtain a good representation of the atmospheric temperature variation along the full VLF propagation path. Thus, we used the MLS temperature data. On the other hand, MLS does not measure NO, therefore the NO data set from SOFIE is used. One key point in the data processing of atmospheric parameters is the separation between daytime and nighttime mesospheric conditions. Since the reflection height of the VLF waves changes between about 70 km during the day to 90 km at night (Thomson et al., 2011, 2014, 2017), we separated the temperature profiles into daytime and nighttime height ranges which were set as 70–75 and 83–88 km, respectively. The same criteria is not applied to the NO profiles because of the large amounts of missing data in those range of altitudes and so, due to this limitation, NO VMR data in the height range of 90–95 km were used for both daytime and nighttime analyses.

2.4. The Wavelet Technique

Wavelet analysis is a tool that decomposes a time series into the time-frequency domain, making it possible to determine both the dominant modes of oscillations (wavelets) and how those modes vary with time (Torrence & Compo, 1998). In this study, the continuous wavelet transform (CWT), XWT, and WTC toolbox for MATLAB package provided by Grinsted et al. (2004) are used, which is available from the URL <http://www.glaciology.net/wavelet-coherence>.

In order to extract the dominant modes, a Morlet function (Morlet et al., 1982) with frequency $w_0 = 6$ and 24 suboctaves per octave (24 voices per power of two) is used. This wavelet function provides a good balance between time and frequency localization (Grinsted et al., 2004). The wavelet transform is complex and thus can be divided into real and imaginary parts or amplitude and phase (Torrence & Compo, 1998). Due to the padding with zeroes employed by the wavelet computation itself, discontinuities are introduced at the end points of every period resulting in errors at the beginning and end of the CWT. These areas are identified using the cone of influence (COI), which is determined in the wavelet analysis (Torrence & Compo, 1998). Thus, wavelet information outside of the COI should be treated with a degree of caution (Torrence & Compo, 1998) whereas within the COI edge effects can be neglected.

Global wavelet power spectra (GWS) are computed by averaging in time the wavelet power spectrum ($|CWT|^2$), in order to determine the significant periods in the whole time series of analysis. XWT can be employed to find regions in the time-frequency domain where two time series show common power via the cross-wavelet distribution (Grinsted et al., 2004). However, the cross-wavelet is unsuitable for significance testing of the interrelation between two processes because the XWT is not normalized (Maraun & Kurths, 2004). As a result, it is also necessary to consider the WTC. The WTC is obtained from the XWT by utilizing a smoothing operator (Liu, 1994; Torrence & Webster, 1999). The WTC is used to measure the degree of local correlation of two series in the time-frequency domain, that is, measure how coherent the XWT is and find significant coherence even if the common power is low. The WTC coefficient is similar to a correlation coefficient with values between 0 and 1, where 0 means no correlation and 1 indicates the strongest possible agreement. WTC is a powerful tool for testing proposed linkages between two time series.

The Monte Carlo method is used to test the significance level of the WTC. Details of this method and XWT, WTC, and the smoothing operator S are given in the literature (e.g., Grinsted et al., 2004; Torrence & Compo,

1998; Torrence & Webster, 1999). In this study, we use the 95% confidence level, which is equivalent to the 5% significance level (Torrence & Compo, 1998).

The wavelet technique demands constant time steps between samples, however some of the time series had a few localized data gaps. In order to allow the wavelet computation we filled those gaps by using their respective smoothed values. The smoothed values were obtained by applying a moving average with a time window length that depends on the maximum length of data gaps of each time series. These maximum lengths are 16, 24, 29, and 35 days for the VLF, temperature, precipitating particle, and NO time series, respectively. This procedure brings the advantage of minimizing the introduction of artifacts in the wavelet analysis.

3. Interrelation Between Periodicities in Subionospheric VLF Variability and Space Weather and Atmospheric Parameters

In this section, the important periods that appear in the VLF variability during daytime and nighttime are retrieved by employing wavelet transform and power spectrum analysis, CWT and GWS (section 3.1). The periods determined are then the focus of further analysis looking at how those relationships change with time. To examine the relation between the VLF variability and selected parameters representing space weather and atmospheric variability the XWT and WTC are computed (section 3.2 for daytime periodicities, and section 3.3 for nighttime). The XWT identifies regions in which common changes in power occur between the time series that are being compared, while the WTC is an accurate representation of the (normalized) covariance between two time series. Thus, in our analysis, if the two evaluated time series are physically related, we expect to find both common power and high levels of coherence in the results.

3.1. Periodicities in Subionospheric VLF Amplitude Data

Figure 3 shows the GWS for the daytime (Figure 3a) and nighttime (Figure 3b) VLF amplitudes in the upper two panels. The dashed lines are the 95% confidence levels for the global wavelet spectrum. Powers above these lines are regarded as significant. The horizontal lines in Figure 3 indicate the maxima of the significant peak periods, that is, those with >95% confidence. The peak periods are identified as 363, 182, 121, and 61 days in the daytime VLF amplitude and 396, 182, 86, 32, and 14 days in the nighttime amplitudes. From those periods, the 363- and 396-day periods can be interpreted as an AO, the 182-day periods as a SAO, and the 32- and 14-day periods as the solar cycle oscillations.

The lower two panels of Figure 3 show the real part of the Morlet wavelet transform for the daytime (Figure 3c) and nighttime (Figure 3d) VLF data. The contours represent the magnitude of the matches between the phases of the wavelet and the time series. In other words, the contour colors indicate the amplitude of the period, from white to red as specified in the color bar. The black curve is the COI, where the values below this curve should be treated with caution. Focusing on the periods indicated by the horizontal lines identified in the power spectrum panels, it can be seen that the daytime AO is well defined in all the years, with a slight decrease in magnitude after 2014 as observed in Figure 2b. The daytime SAO is only well defined in the first half of the study, becoming much weaker from 2013 onward. The 121-day daytime period is not well defined between 2011 and 2015, only showing high wavelet amplitude after 2016. The daytime 61-day period appears every wintertime until 2014, although with a noticeably weaker amplitude in 2011.

The 396-day nighttime period shows a broad peak in the power spectrum, which includes the 365 day period. However, this periodicity shifts in time, exhibiting longer periods during 2013–2014, and splitting into shorter and longer periods after 2015. Thus, while we treat this period as representing the AO, its solar cycle behavior is complex and worthy of future analysis. The nighttime SAO shows the opposite behavior to the daytime SAO, namely, the nighttime SAO increases in magnitude when the daytime SAO vanishes. In particular, the nighttime SAO strengthens around 2010 and after 2014. The nighttime 86-day period is weak for most years, but shows unusually high wavelet amplitude in 2015. The broad peak centered at ~32-day observed in Figure 3d overlaps the ~27 day solar rotation period, which shows high wavelet amplitude intermittently between 2011 and 2016, which are the years of rising, maximum, and declining phase of the solar cycle 24. Similar, but more sporadic occurrence is also observed in the nighttime 14-day period, which has the strongest magnitude in early 2012, late 2016, and 2017.

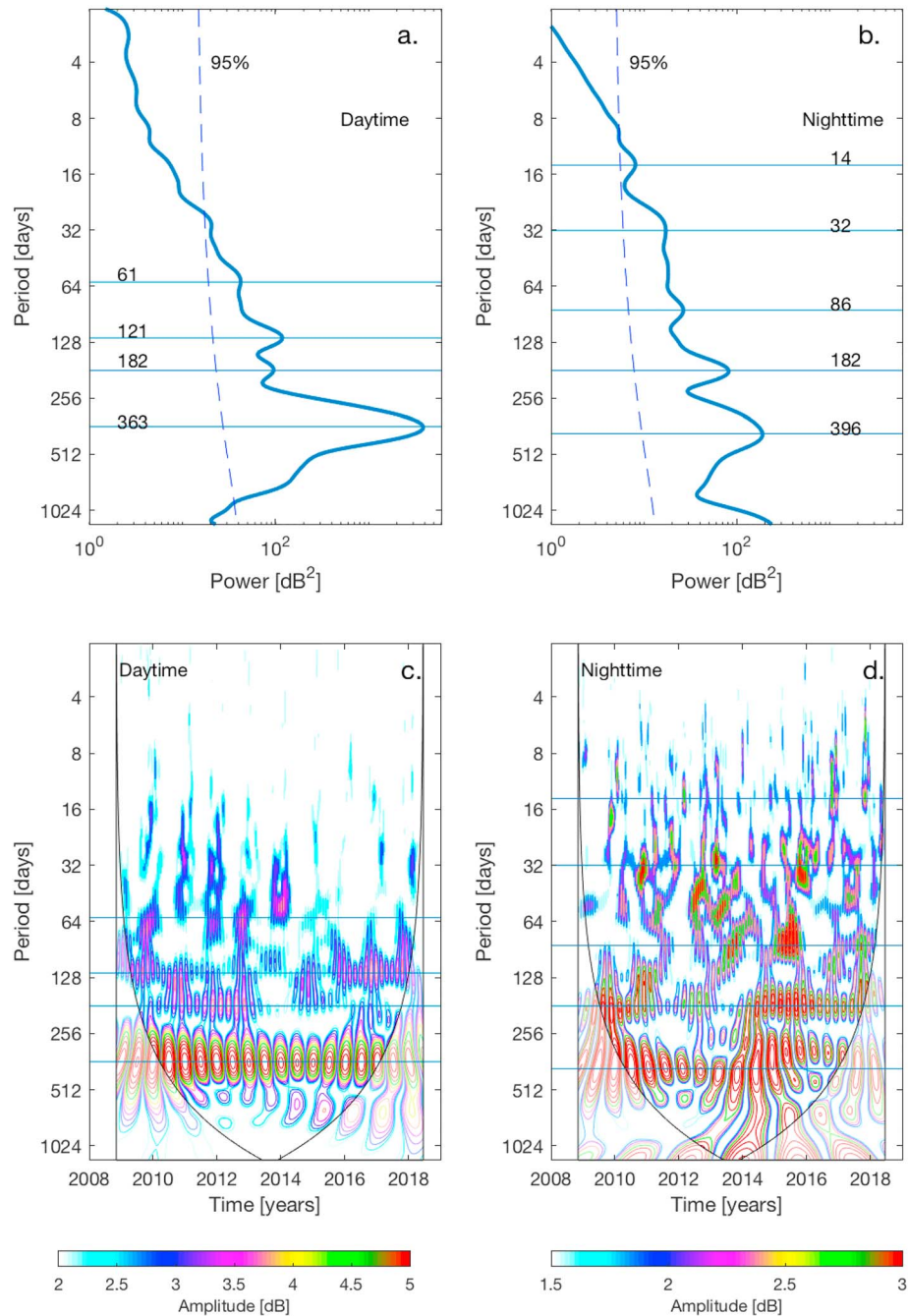


Figure 3. Global wavelet power spectrum of the daytime (a) and nighttime (b) very low frequency amplitude. The dashed line is the 95% confidence level for the global wavelet spectrum. The horizontal lines indicate the peaks of the most significant periods. Contours of the real part of the wavelet transform of the daily daytime (c) and nighttime (d) very low frequency amplitude in the time–period domain. The contours colors indicate the minimum (white) and maximum (red) magnitude of the matches between the phases of the wavelet and the time series. The black curve is the cone of influence.

In general, Figure 3 shows that there are more periodic variations in the nighttime VLF amplitudes than in the daytime data set. This seems reasonable, as the daytime D-region is dominated by solar illumination, while at nighttime other processes can play a significant role in modifying the properties of the D-region. The periodicities undergo changes with time, change in amplitude, and even completely vanish, only to

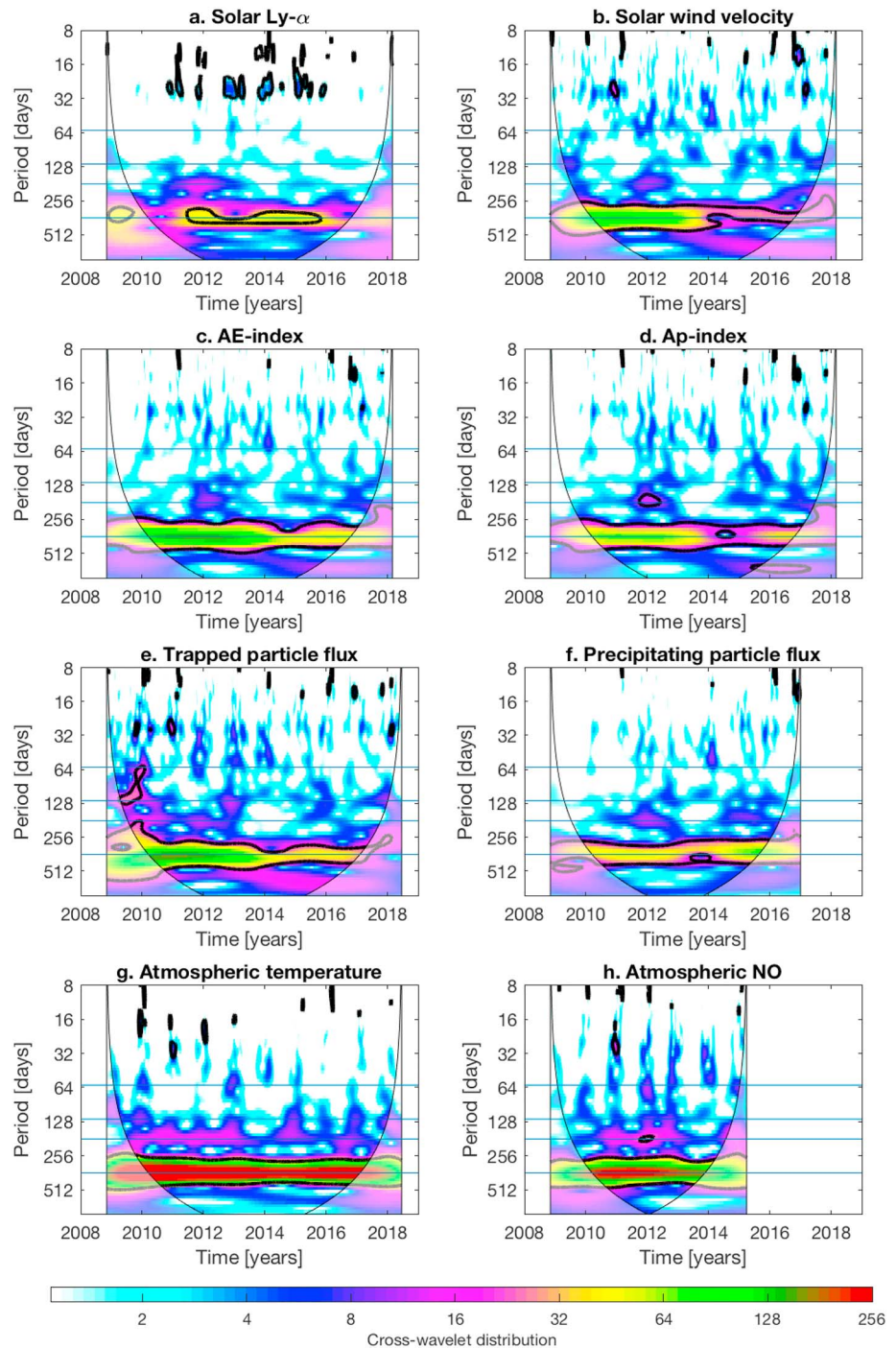


Figure 4. Cross-wavelet distribution for the daytime very low frequency propagation data and solar Ly- α flux (a), solar wind velocity (b), AE index (c), Ap index (d), electron flux at geosynchronous orbit (e), precipitating electron flux (f), atmospheric temperature at 70–75 km (g), and NO volume mixing ratio at 90–95 km (h). The black curve is the cone of influence and the black contours indicate 95% confidence level. The contours colors indicate the high (red) and no (white) significant common powers of two wavelet transform.

reappear some time later. Furthermore, as expected, periodic variations of less than 100 days, that could be connected with the solar rotation oscillation, are also observed. In the next subsections we undertake additional wavelet analysis to provide insights into why these periods might show episodic behavior in the VLF data set and what other physical parameters are related to that behavior.

3.2. Daytime VLF Variability Relations

Figures 4 and 5 are used to identify if the daytime VLF periods of 363- (AO), 182- (SAO), 125-, and 57-days, determined from Figure 3, are associated with periodicities in the selected space weather and atmospheric parameters. Features that appear in Figures 4 and 5 with common power and high levels of coherence could potentially be physically related.

Figure 4 shows the cross-wavelet distribution for the daytime VLF propagation data compared with solar Ly- α flux (a), solar wind velocity (b), *AE* index (c), *Ap* index (d), electron flux at geosynchronous orbit (e), precipitating electron flux (f), atmospheric temperature (g), and NO VMR data (h). The colors indicate the common power of the two wavelet transforms analyzed, ranging from low (white) to high (red). The black curve is the COI that indicates the region below it is potentially influenced by edge effects. The solid black contours indicate 95% confidence level.

Figure 5 shows the WTC for the daytime VLF propagation data compared with the same parameters analyzed in Figure 4. The colors indicate the coherence between the wavelet transform of the two time series. The black curve is the COI, as previously described, and the solid black contours indicate 95% confidence. The arrows represent the relative phase relationship between the two time series analyzed, that is, phase lag. Arrows pointing to the right mean that the two time series are in-phase at a given time, that is, the phase difference is 0° . Arrows pointing to the left mean antiphase, or phase differences of 180° . Arrows pointing downward or upward mean leading or lagging with respect to the in-phase or antiphase. In the analysis we take into account the arrows of those periods above 64-day because of the clear phase lag feature inside the 95% confidence level. Arrows are only plotted when the confidence areas are large enough to show them clearly. Furthermore, we expect a consistent or slowly varying phase lag when the two analyzed time series are physically related.

Common constant power and coherence of the daytime AO is observed over all the analyzed years for atmospheric temperature in the 70–75 km altitude range and NO in the 90–95 km altitude range. The relation is strong with a constant phase difference of 180° , represented by the arrows pointing to the left, which indicates that the VLF and the mesospheric variabilities are in antiphase. The solar wind, geomagnetic, and particle variability analysis with the VLF AO variability shows a clear weakening in the power after 2014. This finding could be also related to the weakening VLF amplitude observed after 2014 in Figures 2b and 3a. The coherence also fades around 2014. In this case, the lack of coherence is directly associated with the prominent change in the phase, of $\sim 180^\circ$, between the VLF and space weather periodicities, indicated by the arrows before and after 2014. Ly- α solar radiation only shows common power in the AO around the years of solar maximum.

Despite showing high amplitude SAO influence in the pre-2014 VLF daytime analysis in Figure 3, there is little evidence of common power and coherence coming from the parameters analyzed in Figures 4 and 5. The SAO is clearly related to the *Ap* index and NO variabilities around 2012. Additional and less evident relationships are observed before 2013 with particle precipitation and atmospheric temperature. Notably, their arrows in the WTC analysis do not point to the same direction, which could indicate that different and independent processes could be taking place that are not included in this analysis.

Figures 4 and 5 show that the 121- and 61-day periods observed in the daytime VLF data are not clearly related to any of the space weather or atmospheric parameters considered in this study. On the other hand, and contrary to the GWS results shown in Figure 3 where periods shorter than 64 days are insignificant, the XWT and WTC reveal intermittent significant correlation at ~ 27 - and ~ 14 -day periods. These periods are particularly observed with the Ly- α solar radiation and very weakly with solar wind, geomagnetic activity, and particles. In addition, periods shorter than 64-day are observed especially during winter time with the atmospheric parameters, which suggests a possible role of planetary waves in the modulation of the VLF variability.

In brief, the daytime AO is consistently related to mesospheric temperature and NO variabilities. The daytime SAO appears to be mainly related to the *Ap* index and NO, although the connection is likely to be complicated by weak associations with other solar, geomagnetic, and atmospheric parameters. Shorter solar rotation oscillations show up clearly in this analysis. As a whole, the daytime VLF periods are related to complex combinations of space weather and atmospheric variations at different phases of the solar cycle.

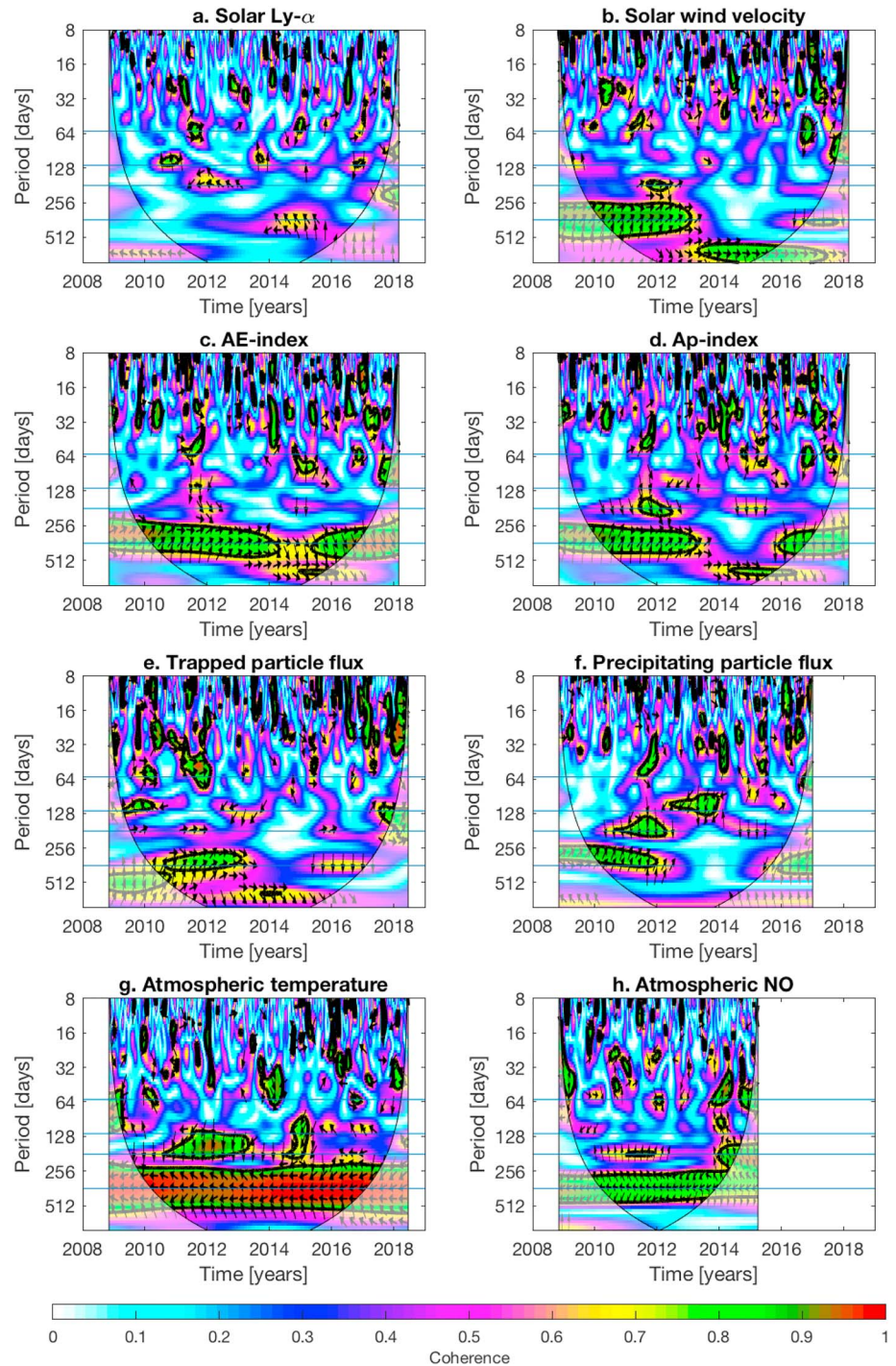


Figure 5. Square wavelet coherency for the daytime very low frequency propagation data and solar Ly- α flux (a), solar wind velocity (b), AE index (c), Ap index (d), electron flux at geosynchronous orbit (e), precipitating electron flux (f), atmospheric temperature at 70–75 km (g), and NO volume mixing ratio at 90–95 km (h). The black curve is the cone of influence and the solid black contours indicate 95% confidence level. The contours colors indicate no correlation (white) and high correlation (red) between the two wavelet transform. The relative phase relationship is shown as arrows. Arrows pointing to the right or to the left mean in-phase and antiphase, respectively.

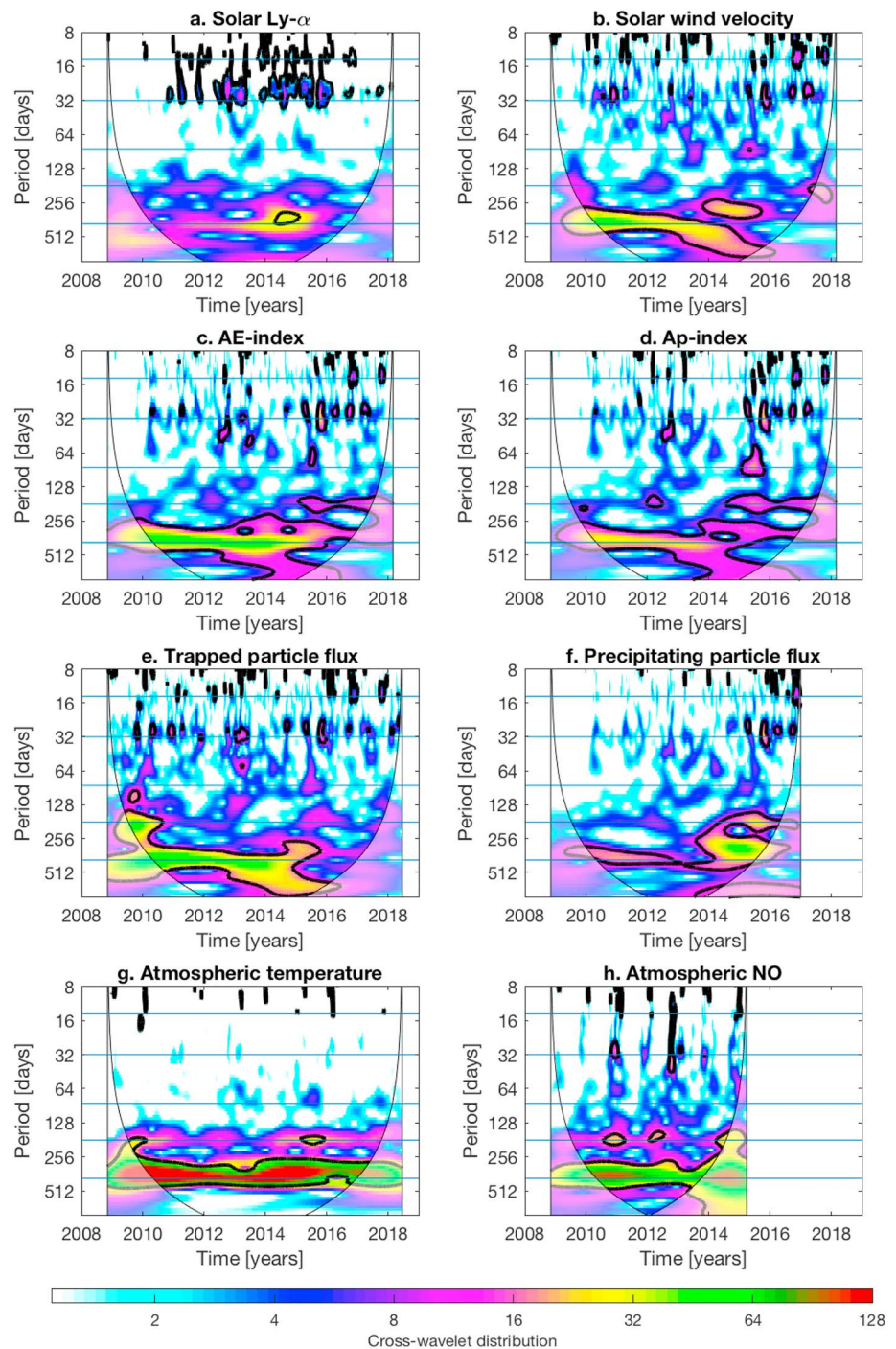


Figure 6. As described in Figure 4 but for the nighttime very low frequency propagation data. For the analysis the atmospheric temperature at 83–87 km was used.

3.3. Nighttime VLF Variability Relations

Figures 6 and 7 are the same format as Figures 4 and 5, but for the nighttime VLF propagation signal, that is, the cross-wavelet and WTC analysis. The nighttime analysis suggests that the VLF periods of 396- (AO), 182- (SAO), 86-, and 32- and 14-day (solar rotation oscillations) determined from Figure 3 can be related to different combinations of space weather and atmospheric variations at various times, often changing as the solar cycle phase changes. This is a similar finding to those of the daytime analysis.

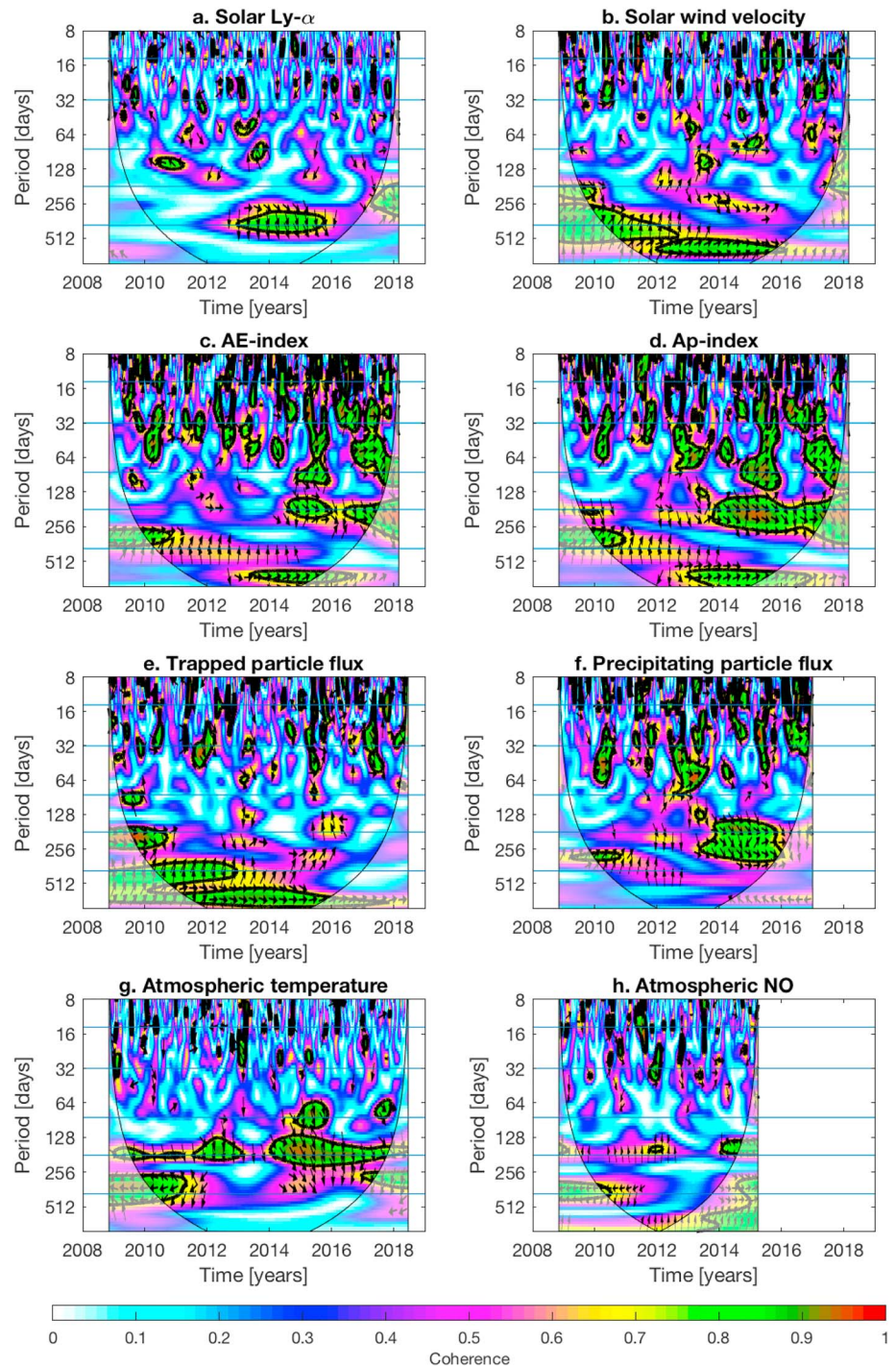


Figure 7. As described in Figure 5 but for the nighttime very low frequency propagation data. For the analysis the atmospheric temperature at 83–87 km was used.

Whereas the mesospheric temperature strongly dominates the nighttime AO in common power shown in Figure 6, there is no significant coherence with the VLF variability within the COI in Figure 7 apart from an antiphase relationship up to 2012. This result suggests that atmospheric variability is not clearly related to the annual variability of nighttime VLF amplitudes during most of the years in the study. However, Figures 6 and 7 show that the nighttime AO is related to solar wind, geomagnetic indices, and particle

fluxes up until the solar maximum in 2014. Ly- α can be considered as the dominant driver of nighttime VLF variability on annual time scales during the solar cycle maximum (2014–2016).

The XWT and WTC of Figures 6 and 7, respectively, show that the nighttime SAO has a permanent weak relation to mesospheric temperature and NO. Hence, this weak relation can be considered as a background level of the SAO. The post-2014 increase in SAO nighttime VLF amplitude shown in Figure 3 appears to be related to common power and coherence in geomagnetic activity, and precipitating particle flux parameters. In addition, comparing this result with that of the daytime analysis, we find that enhancements in the magnitude of SAO are related to the geomagnetic activity in both nighttime and daytime VLF amplitudes.

Figures 6 and 7 show that significant common power and coherence of the 86-day periodicity is primarily related to geomagnetic activity. This match only occurs during the beginning of the declining phase of the sunspot solar cycle, that is, 2015, and appears to be primarily in-phase. In the case of the solar rotation oscillations (27 and 14 days) observed in the nighttime VLF amplitude, Figures 6 and 7 show that they are most clearly linked with Ly- α solar radiation in common power and geomagnetic indexes and particle fluxes in coherency analysis. The analysis with solar wind, geomagnetic indices, and precipitating particles show increased common power from about 2015, in other words, during the declining phase of the solar cycle.

To condense, nighttime VLF amplitudes show more relationship with solar and geomagnetic parameters than during the daytime. However, for the AO and SAO periodicities weak influences of atmospheric temperature and NO remain.

4. Discussion

In this study, periodic variations due to space weather and atmospheric activity induced in daytime and nighttime high-latitude VLF measurements are examined by wavelet analysis. The amplitude of the VLF signal emitted by the NAA transmitter recorded in Finland is used to find the significant periodicities. Those periods are 363, 182, 121, and 61 days in the daytime VLF amplitude, and 396, 182, 86, and 32 and 14 days in the nighttime amplitudes. The 396- and 363-day periods can be interpreted as the AO, the 182-day period as the SAO, and the 32- and 14-day periods as the solar rotation oscillations.

The present study shows that there are more different periodicities in the nighttime VLF amplitude variability than in daytime. This result is expected because during daytime solar illumination is the main source of ionization that controls signal variability, decreasing the D-region ionospheric sensitivity to other external sources (Macotela et al., 2017). During nighttime, when direct solar illumination influence is excluded, the ionospheric sensitivity to other drivers increases (Raulin et al., 2014) allowing a wider range of physical and chemical processes to influence VLF propagation conditions. But nevertheless, the common periodicities observed during both daytime and nighttime are the AO and SAO. To facilitate the comparison of the GWS of the daytime and nighttime VLF amplitudes, each GWS is normalized to its variance (Torrence & Compo, 1998). By this computation we find that the daytime AO power is ~ 2.5 that of the nighttime AO. An opposite effect occurs for the SAO. In this case, the nighttime SAO exhibits ~ 7.5 times more power than during the daytime. A higher AO during daytime and a higher SAO during nighttime was also found by Sharma et al. (2017) using a subpolar VLF path. This agreement suggests that this common feature could be a characteristic of AO/SAO periodicities in the polar regions.

The strongest relationship exhibited by the daytime AO is to antiphase mesospheric temperature and antiphase NO, which is consistently antiphase. The mesospheric temperature result matches the finding of Silber et al. (2013) who explained the common variability through global seasonal solar irradiance changes. The most significant nighttime AO driver is Ly- α radiation, showing increasing power, and high coherence, around the maximum of the solar cycle. This last result confirms that geo-coronal Ly- α is the main source of ionizing radiation at night of neutral NO (Banks & Kockarts, 1973). Up until 2014, that is, at the time of the solar cycle maximum, analysis of daytime and nighttime AO with solar wind, geomagnetic activity, and particle flux parameters exhibit high levels of common power and coherence. A change in both amplitude and phase of the AO occurred around 2014. The change in amplitude can be understood in terms of the Rosenberg-Coleman effect (Rosenberg & Coleman, 1969) of dominant interplanetary magnetic field (IMF) polarities. Echer and Svalgaard (2004) found that the annual variation in the IMF polarity is constrained to the rising phase of solar cycles, and they explained this asymmetry by the more stable and flat

heliospheric current sheet that is present only in the rising phase of solar cycles. In addition, Zieger and Mursula (1998) reported a similar behavior of the annual variations of solar wind, geomagnetic activity, and IMF. Thus, the high power of AO observed before 2014 in the VLF measurements could be a combination of the annual solar radiation change and the Rosenberg-Coleman effect.

The daytime and nighttime SAO relation to geomagnetic activity and particle fluxes could be explained by the semiannual variation in geomagnetic activity (Svalgaard, 2011). Using Figure 1 of Zhao and Zong (2012), and according to the method we use to differentiate between daytime and nighttime variability, we can apply the Russell-McPherron effect (Russell & McPherron, 1973) and the equinoctial hypothesis, respectively, to explain the SAO observed in the VLF amplitude variations. The main difference between these two semiannual variations is that the equinoctial hypothesis is related to modulation of the existing geomagnetic activity, while the Russell-McPherron effect is producing the geomagnetic activity (Svalgaard, 2011). However, both semiannual variations occur at the same time, and both mechanisms connect to the VLF amplitude oscillations via geomagnetic activity and electron precipitation. The differences in the observations before and after 2014 could be connected with the ~22 year variation in geomagnetic activity (Cliver et al., 2004; Svalgaard, 2011). This interesting result showing the swap of the SAO influence on the D-region from daytime to nighttime in different phases of the solar cycle, deserves further investigation in a future study.

In the case of the 121 and 61-day periods observed during daytime, we found that these periodicities are not clearly associated with the space weather and atmospheric parameters analyzed in this study, that is, they are only observed in the VLF time series. However, Bai (2003) found a 129-day periodicity in solar flare occurrence. Similarly, Kilcik et al. (2010) obtained the 62-day period as one of the prominent solar flare periodicities for solar cycle 23. We did not consider solar flare analysis in this study but it is very well known that the lower ionosphere is strongly affected by this kind of solar event (Thomson et al., 2005).

The 86-day period observed during nighttime VLF amplitudes in 2015 is clearly related to the Ap index. This periodicity was not reported in previous studies (e.g., Clúa de Gonzalez et al., 1993). We undertook additional wavelet analysis to verify if the 86-day period appears during other solar cycles. For that we used the Ap index data from 1963–2018, that is, covering five solar cycles, from the OMNIWEB data base. We found that the 86-day period appears with strong power mainly during the maximum and declining phase of solar cycles, which is consistent with the periodic variation in the VLF measurements during the declining phase of solar cycle 24 reported in the present study.

The solar rotation oscillation, and its first harmonic, observed in the VLF measurements can be linked to direct Ly- α radiation during daytime, and scattered Ly- α radiation for the nighttime lower ionosphere (Strobel, 1974). The variability of the quiescent Ly- α emission during a solar rotation is between 5% and 40% of its background level (Lean & Skumanich, 1983). A 40% increase in the Ly- α flux would produce measurable variations in the lower ionosphere and be detected by subionospherically propagating VLF waves (Raulin et al., 2013).

The solar rotation oscillation seen in the relationship of VLF amplitudes with geomagnetic activity observed during the declining phase of the solar cycle may be explained by three mechanisms. First, the active regions (sunspots) and their magnetic fields are better organized and more long-lived during the maximum and declining portion of solar cycle than during its rising portion (Pap et al., 1990). Second, during years with antiparallel solar magnetic field there are more geoeffective events (Baranyi & Ludmány, 2003). The antiparallel years started in 2015 which coincide with the observed association between 27-day period VLF amplitudes and geomagnetic activity. Third, modulation of the solar wind interaction with the Earth's magnetic field, due to high-speed streams (Krieger et al., 1973), which maximize during the declining phase of the solar cycle (Hakamada & Akasofu, 1981). Furthermore, high-speed streams have the largest relative effect on geomagnetic activity at the high-latitude polar paths studied here (Finch et al., 2008).

Although the wavelet transform of the daytime VLF amplitudes did not show any significant power at periods of 27 days, a broad peak in nighttime VLF amplitudes was found at 32 days. Additional common power and coherence analysis with solar, geomagnetic, and atmospheric parameters identify the influence of the 27-day solar rotation oscillation, but fails to explain why there should be significant power at slightly longer periods than this, resulting in the observed peak at 32 days in the nighttime analysis. In order to explain this result we hypothesize that the measured VLF nighttime signal amplitudes also contain the influences of

external physical sources that are not clearly observed in our analysis. Atmospheric planetary waves with periods of 30 days or more have been detected using partial reflections of medium frequency radar signals at altitudes in the range 65–110 km (Manson et al., 1981). These atmospheric Rossby waves influence pressures in the mesosphere and hence could modify the VLF reflection height, thus changing the radio wave propagation conditions and received signals. Further analysis is required to test this hypothesis. On the other hand, there is the possibility of a lunar influence, with 28-day periodicity, on nighttime electron densities in the D-region, as was observed by Friedrich et al. (2011) using rocket sounding measurements.

One way to study atmospheric waves is by means of the temperature parameter. However, the coherence and cross-correlation analysis between the VLF amplitude data and the atmospheric temperature do not show important periods below 32 days. Thus, as a further study, it would be interesting to analyze only the winter time periods, because it has been shown that planetary waves can be more important during the winter season (McDonald et al., 2011).

5. Conclusions

In this paper we have retrieved the important periods that appear in daytime and nighttime VLF radio wave amplitude variability by employing wavelet techniques. The relation of those periods to eight selected space weather and atmospheric parameters has been found using cross-wavelet and WTC analysis. We found that more significant periods are observed during nighttime than during daytime analysis. Our results show

1. AO in daytime VLF amplitudes is in antiphase with mesospheric temperature variations, while the nighttime AO is more strongly influenced by Ly- α flux variability.
2. SAO in daytime VLF amplitudes occur only prior to solar maximum and show similar periodicities to geomagnetic activity. Conversely, nighttime SAO only occur after solar maximum, but is also related to geomagnetic activity variations.
3. Quasi 27-day solar rotation oscillation in nighttime VLF amplitudes are dominated by Ly- α variability at solar maximum, and geomagnetic activity during the declining phase.
4. Periods that occur in the VLF amplitudes of ~30–120 days are transient. Some periodicities (~100 days) could be associated with solar flare occurrence, and others (~30 days) appear to be driven by other factors, for example, planetary wave activity.

Our results are important since the VLF signals are related to periodic variations of electron density in the D-region ionosphere and have been used to identify the processes that influence the behavior of the upper atmosphere. These results can provide useful constraints on the long-term and short-term variability in coupled ion-neutral atmospheric models, thereby adding to our understanding of the response of the chemistry, dynamics, and electrodynamics of the Earth's ionosphere to solar and atmospheric forcing. Finally, it would be relevant to evaluate the periodic variations that affect the VLF measurements using VLF paths at other regions of the Earth, as those monitored by the AARDDVARK network.

Acknowledgments

E.L.M. was supported by the Suomen Kulttuurirahasto (grant 00170658) and the Tauno Tönnöningin Säätiö (grant 20170007). D.A.N. and M.A.C. were supported in part by the Natural Environment Research Council (grant NE/J022187/1). Data availability is described at the following websites: <http://www.sgo.fi/Data/VLF/VLF.php> (AARDDVARK), <https://omniweb.gsfc.nasa.gov/form/dx1.html> (OMNI database), <https://umbra.nascom.nasa.gov/sdb/goes/particle/> (GOES particle), https://mls.jpl.nasa.gov/products/temp_product.php (EOS MLS), <http://sofie.gats-inc.com/sofie/index.php> (SOFIE AIM).

References

- Aguilar-Rodríguez, E., Rodríguez-Martínez, M., Romero-Hernández, E., Mejía-Ambríz, J. C., González-Esparza, J. A., & Tokumaru, M. (2014). The wavelet transform function to analyze interplanetary scintillation observations. *Geophysical Research Letters*, *41*, 3331–3335. <https://doi.org/10.1002/2014GL060047>
- Bai, T. (2003). Periodicities in solar flare occurrence: Analysis of cycles 19–23. *The Astrophysical Journal*, *591*(1), 406–415. <https://doi.org/10.1086/375295>
- Banks, P. M., & Kockarts, G. (1973). *Aeronomy, Part A*, 430. U. S.: Academic Press.
- Baranyi, T., & Ludmány, A. (2003). Effects of solar polarity reversals on geoeffective plasma streams. *Journal of Geophysical Research*, *108*(A5), 1212. <https://doi.org/10.1029/2002JA009553>
- Bracewell, R. N., & Straker, T. W. (1949). The study of solar flares by means of very long radio waves. *Monthly Notices of the Royal Astronomical Society*, *109*, 28–45. <https://doi.org/10.1093/mnras/109.1.28>
- Callis, L. B., Baker, D. N., Blake, J. B., Lambeth, J. D., Boughner, R. E., Natarajan, M., Klebesadel, R. W., et al. (1991). Precipitating relativistic electrons: Their long-term effect on stratospheric odd nitrogen levels. *Journal of Geophysical Research*, *96*, 2939–2976. <https://doi.org/10.1029/90JD02184>
- Clilverd, M. A., Rodger, C. J., Brundell, J., Bähr, J., Cobbett, N., & Moffat-Griffin, T., et al. (2008). Energetic electron precipitation during substorm injection events: High-latitude fluxes and an unexpected midlatitude signature. *Journal of Geophysical Research*, *113*, A10311. <https://doi.org/10.1029/2008JA013220>
- Clilverd, M. A., Rodger, C. J., Dietrich, S., Raita, T., Ulich, T., Clarke, E., Thomson, A. W. P., et al. (2010). High-latitude geomagnetically induced current events observed on very low frequency radio wave receiver systems. *Radio Science*, *45*, RS2006. <https://doi.org/10.1029/2009RS004215>
- Clilverd, M. A., Rodger, C. J., Thomson, N. R., Brundell, J. B., Ulich, T., Lichtenberger, J., Cobbett, N., et al. (2009). Remote sensing space weather events: Antarctic-Arctic radiation-belt (dynamic) deposition-VLF Atmospheric Research Consortium network. *Space Weather*, *7*, 804001. <https://doi.org/10.1029/2008SW000412>

- Cliver, E. W., Svalgaard, L., & Ling, A. G. (2004). Origins of the semiannual variation of geomagnetic activity in 1954 and 1996. *Annales Geophysicae*, 22, 93–100. <https://doi.org/10.5194/angeo-22-93-2004>
- Clúa de Gonzalez, A. L., Gonzalez, W. D., Dutra, S. L. G., & Tsurutani, B. T. (1993). Periodic variation in the geomagnetic activity: A study based on the Ap index. *Journal of Geophysical Research*, 98, 9215–9231. <https://doi.org/10.1029/92JA02200>
- Demirkol, M. K., Inan, U. S., Bell, T. F., Kanekal, S. G., & Wilkinson, D. C. (1999). Ionospheric effects of relativistic electron enhancement events. *Geophysical Research Letters*, 26, 3557–3560. <https://doi.org/10.1029/1999GL010686>
- Echer, E., & Svalgaard, L. (2004). Asymmetry in the Rosenberg-Coleman effect around solar minimum revealed by wavelet analysis of the interplanetary magnetic field polarity data (1927–2002). *Geophysical Research Letters*, 31, L12808. <https://doi.org/10.1029/2004GL020228>
- Evans, D. S., & Greer, M. S. (2004). Polar-orbiting environmental satellite space environment monitor-2 instrument descriptions and archive data documentation. NOAA Tech. Memorandum version 1.4, Space Environment Laboratory, Colo.
- Finch, I. D., Lockwood, M. L., & Rouillard, A. P. (2008). Effects of solar wind magnetosphere coupling recorded at different geomagnetic latitudes: Separation of directly-driven and storage/release systems. *Geophysical Research Letters*, 35, L21105. <https://doi.org/10.1029/2008GL035399>
- Friedrich, M., Rapp, M., Plane, J., & Torkar, K. (2011). Bite-outs and other depletions of mesospheric electrons. *Journal of Atmospheric and Solar-Terrestrial Physics*, 73, 2201–2211. <https://doi.org/10.1016/j.jastp.2010.10.018>
- Gordley, L. L., Hervig, M. E., Fish, C., Russell, J. M., Bailey, S., Cook, J., Hansen, S., et al. (2009). The Solar Occultation For Ice Experiment (SOFIE). *Journal of Atmospheric and Solar-Terrestrial Physics*, 71, 300–315. <https://doi.org/10.1016/j.jastp.2008.07.012>
- Grinsted, A., Moore, J. C., & Jevrejeva, S. (2004). Application of the cross wavelet transform and wavelet coherence to geophysical time series. *Nonlinear Processes in Geophysics*, 11, 561–566. <https://doi.org/10.5194/npg-11-561-2004>
- Hakamada, K., & Akasofu, S.-I. (1981). A cause of solar wind speed variations observed at 1 AU. *Journal of Geophysical Research*, 86, 1290–1298. <https://doi.org/10.1029/JA086iA03p01290>
- Hargreaves, J. K. (1992). *The solar-terrestrial environment*. New York: Cambridge University Press. <https://doi.org/10.1017/CBO9780511628924>
- Kilcik, A., Ozguc, A., Rozelot, J. P., & Atac, T. (2010). Periodicities in solar flare index for cycles 21–23 revisited. *Solar Physics*, 264(1), 255–268. <https://doi.org/10.1007/s11207-010-9567-7>
- Krieger, A. S., Timothy, A. F., & Roelof, E. C. (1973). A coronal hole and its identification as the source of a high velocity solar wind stream. *Solar Physics*, 29, 505–525. <https://doi.org/10.1007/BF00150828>
- Kumar, S., NaitAmor, S., Chanrion, O., & Neubert, T. (2017). Perturbations to the lower ionosphere by tropical cyclone Evan in the South Pacific Region. *Journal of Geophysical Research: Space Physics*, 122, 8720–8732. <https://doi.org/10.1002/2017JA024023>
- Lam, M. M., Horne, R. B., Meredith, N. P., Glauert, S. A., Moffat-Griffin, T., & Green, J. C. (2010). Origin of energetic electron precipitation >30 keV into the atmosphere. *Journal of Geophysical Research*, 115, A00F08. <https://doi.org/10.1029/2009JA014619>
- Lean, J. L., & Skumanich, A. (1983). Variability of the Lyman alpha flux with solar activity. *Journal of Geophysical Research*, 88, 5751–5759. <https://doi.org/10.1029/JA088iA07p05751>
- Liu, P. C. (1994). Wavelet spectrum analysis and ocean wind waves. In E. Foufoula-Georgiou & P. Kumar (Eds.), *Wavelets in geophysics, Wavelet Analysis and Its Applications* (pp. 151–166). San Diego, CA: Academic Press. <https://doi.org/10.1016/B978-0-08-052087-2.50012-8>
- Livesey, N., Read, W., Wagner, P., Froidevaux, L., Lambert, A., Manney, G., et al. (2017). Version 4.2x level 2 data quality and description document, Version 4.2x-3.1. Pasadena, CA: Jet Propulsion Laboratory. Retrieved from https://mls.jpl.nasa.gov/data/v4-2_data_quality_document.pdf
- Macotela, E. L., Raulin, J.-P., Manninen, J., Correia, E., Turunen, T., & Magalhães, A. (2017). Lower ionosphere sensitivity to solar X-ray flares over a complete solar cycle evaluated from VLF signal measurements. *Journal of Geophysical Research: Space Physics*, 122, 12,370–12,377. <https://doi.org/10.1002/2017JA024493>
- Manson, A. H., Meek, C. E., & Gregory, J. B. (1981). Winds and wave (10 min–30 days) in the mesosphere and lower thermosphere at Saskatoon (52°N, 107°W, L = 4.3) during the year, October 1979 to July 1980. *Journal of Geophysical Research*, 86, 9615–9625. <https://doi.org/10.1029/JC086iC10p09615>
- Maraun, D., & Kurths, J. (2004). Cross wavelet analysis: Significance testing and pitfalls. *Nonlinear Processes in Geophysics*, 11(4), 505–514. <https://doi.org/10.5194/npg-11-505-2004>
- Maurya, A. K., Phanikumar, D. V., Singh, R., Kumar, S., Veenadhari, B., Kwak, Y.-S., Kumar, A., et al. (2014). Low-mid latitude D region ionospheric perturbations associated with 22 July 2009 total solar eclipse: Wave-like signatures inferred from VLF observations. *Journal of Geophysical Research: Space Physics*, 119, 8512–8523. <https://doi.org/10.1002/2013JA019521>
- McDonald, A. J., Hibbins, R. E., & Jarvis, M. J. (2011). Properties of the quasi 16 day wave derived from EOS MLS observations. *Journal of Geophysical Research*, 116, D06112. <https://doi.org/10.1029/2010JD014719>
- McWilliams, A., & Strait, K. (1976). Recurrent VLF amplitude fluctuations: Detection using a filter and correspondence with geomagnetic disturbances. *Journal of Geophysical Research*, 81, 2423–2428. <https://doi.org/10.1029/JA081i013p02423>
- Morlet, J., Arens, G., Fourgeau, E., & Glard, D. (1982). Wave propagation and sampling theory—Part I: Complex signal and scattering in multilayered media. *Geophysics*, 47(2), 203–221. <https://doi.org/10.1190/1.1441328>
- Neal, J. J., Rodger, C. J., Clilverd, M. A., Thomson, N. R., Raita, T., & Ulich, T. (2015). Long-term determination of energetic electron precipitation into the atmosphere from AARDDVARK subionospheric VLF observations. *Journal of Geophysical Research: Space Physics*, 120, 2194–2211. <https://doi.org/10.1002/2014JA020689>
- Nicolet, M. E., & Aikin, A. C. (1960). The formation of the D region of the ionosphere. *Journal of Geophysical Research*, 65, 1469–1483. <https://doi.org/10.1029/JZ065i005p01469>
- Onsager, T. G., Grubb, R., Kunches, J., Matheson, L., Speich, D., Zwickl, R., & Sauer, H. (1996). Operational uses of the GOES energetic particle detectors. In E. R. Washwell (Ed.), *GOES-8 and Beyond* (Vol. 2812, 281 pp.). Denver, CO: Proc. SPIE Int. Soc. Opt. Eng., 2812, 281.
- Pal, S., Chakraborty, S., & Chakrabarti, S. (2015). On the use of very low frequency transmitter data for remote sensing of atmospheric gravity and planetary waves. *Advances in Space Research*, 55, 1190–1198. <https://doi.org/10.1016/j.asr.2014.11.023>
- Pap, J., Tobiska, W. K., & Bouwer, S. D. (1990). Periodicities of solar irradiance and solar activity indices, I. *Solar Physics*, 129(1), 165–189. <https://doi.org/10.1007/BF00154372>
- Raulin, J.-P., Trottet, G., Giménez de Castro, C. G., Correia, E., & Macotela, E. L. (2014). Nighttime sensitivity of ionospheric VLF measurements to X-ray bursts from a remote cosmic source. *Journal of Geophysical Research: Space Physics*, 119, 4758–4766. <https://doi.org/10.1002/2013JA019670>

- Raulin, J.-P., Trottet, G., Kretschmar, M., Macotela, E. L., Pacini, A., Bertoni, F. C. P., & Dammasch, I. E. (2013). Response of the low ionosphere to X-ray and Lyman- α solar flare emissions. *Journal of Geophysical Research: Space Physics*, *118*, 570–575. <https://doi.org/10.1029/2012JA017916>
- Rodger, C. J., Kavanagh, A. J., Clilverd, M. A., & Marple, S. R. (2013). Comparison between POES energetic electron precipitation observations and riometer absorptions: Implications for determining true precipitation fluxes. *Journal of Geophysical Research: Space Physics*, *118*, 7810–7821. <https://doi.org/10.1002/2013JA019439>
- Rosenberg, R. L., & Coleman, P. J. (1969). Heliographic latitude dependence of dominant polarity of interplanetary magnetic field. *Journal of Geophysical Research*, *74*, 5611–5622. <https://doi.org/10.1029/JA074i024p05611>
- Russell, C. T., & McPherron, R. L. (1973). Semiannual variation of geomagnetic activity. *Journal of Geophysical Research*, *78*, 92–108. <https://doi.org/10.1029/JA078i001p00092>
- Samanes, J., Raulin, J. P., Cao, J., & Magalhaes, A. (2018). Nighttime lower ionosphere height estimation from the modal interference distance. *Journal of Atmospheric and Solar-Terrestrial Physics*, *167*, 39–47. <https://doi.org/10.1016/j.jastp.2017.10.009>
- Sharma, G., Kandel, K., Khadka, B., Schnoor, P., Bhatta, K., Ghimire, B., & Thapa, A. (2017). A study on the VLF/LF long term amplitude oscillations associated with frequencies 37.5 kHz and 45.9 kHz received at Keil Longwave Monitor, Keil, Germany. *International Journal of Geosciences*, *08*(09), 1080–1090. <https://doi.org/10.4236/ijg.2017.89061>
- Silber, I., Price, C., & Rodger, C. (2016). Semi-annual oscillation (SAO) of the nighttime ionospheric D region as detected through ground-based VLF receivers. *Atmospheric Chemistry and Physics*, *16*, 3279–3288. <https://doi.org/10.5194/acp-16-3279-2016>
- Silber, I., Price, C., Rodger, C. J., & Haldoupis, C. (2013). Links between mesopause temperatures and ground-based VLF narrowband radio signals. *Journal of Geophysical Research: Atmospheres*, *118*, 4244–4255. <https://doi.org/10.1002/jgrd.50379>
- Simon Wedlund, M., Clilverd, M. A., Rodger, C. J., Cresswell-Moorcock, K., Cobbett, N., Breen, P., et al. (2014). A statistical approach to determining energetic outer radiation-belt electron precipitation fluxes. *Journal of Geophysical Research: Space Physics*, *119*, 3961–3978. <https://doi.org/10.1002/2013JA019715>
- Strobel, D. F. (1974). Physics and chemistry of the E region: A review. *Radio Science*, *9*, 159–165. <https://doi.org/10.1029/RS009i002p00159>
- Svalgaard, L. (2011). Geomagnetic semiannual variation is not overestimated and is not an artifact of systematic solar hemispheric asymmetry. *Geophysical Research Letters*, *38*, L16107. <https://doi.org/10.1029/2011GL048616>
- Thomson, N., & Clilverd, M. (2000). Solar cycle changes in daytime VLF subionospheric attenuation. *Journal of Atmospheric and Solar-Terrestrial Physics*, *62*(7), 601–608. [https://doi.org/10.1016/S1364-6826\(00\)00026-2](https://doi.org/10.1016/S1364-6826(00)00026-2)
- Thomson, N. R., Clilverd, M. A., & Rodger, C. J. (2014). Low latitude Ionospheric D-region dependence on solar zenith angle. *Journal of Geophysical Research: Space Physics*, *119*, 6865–6875. <https://doi.org/10.1002/2014JA020299>
- Thomson, N. R., Clilverd, M. A., & Rodger, C. J. (2017). Midlatitude ionospheric D region: Height, sharpness and solar zenith angle. *Journal of Geophysical Research: Space Physics*, *122*, 8933–8946. <https://doi.org/10.1002/2017JA024455>
- Thomson, N. R., Clilverd, M. A., & Rodger, C. J. (2018). Quiet daytime Arctic ionospheric D region. *Journal of Geophysical Research: Space Physics*, *123*, 9726–9742. <https://doi.org/10.1029/2018JA025669>
- Thomson, N. R., Rodger, C. J., & Clilverd, M. A. (2005). Large solar flares and the ionospheric D-region enhancements. *Journal of Geophysical Research*, *110*, A06306. <https://doi.org/10.1029/2005JA011008>
- Thomson, N. R., Rodger, C. J., & Clilverd, M. A. (2011). Daytime D-region parameters from long path VLF phase and amplitude. *Journal of Geophysical Research*, *116*, A11305. <https://doi.org/10.1029/2011JA016910>
- Thorne, R. M., & Larsen, T. R. (1976). An investigation of relativistic electron precipitation events and their association with magnetic substorm activity. *Journal of Geophysical Research*, *81*, 5501–5506. <https://doi.org/10.1029/JA081i031p05501>
- Torrence, C., & Compo, G. (1998). A practical guide to wavelet analysis. *Bulletin of the American Meteorological Society*, *79*, 61–78. [https://doi.org/10.1175/1520-0477\(1998\)079<0061:APGTWA>2.0.CO;2](https://doi.org/10.1175/1520-0477(1998)079<0061:APGTWA>2.0.CO;2)
- Torrence, C., & Webster, P. J. (1999). Interdecadal changes in the ENSO-monsoon system. *Journal of Climate*, *12*, 2679–2690. [https://doi.org/10.1175/1520-0442\(1999\)012<2679:ICITEM>2.0.CO;2](https://doi.org/10.1175/1520-0442(1999)012<2679:ICITEM>2.0.CO;2)
- Turunen, E., Verronen, P. T., Seppälä, A., Rodger, C. J., Clilverd, M. A., Tamminen, J., Enell, C. F., et al. (2009). Impact of different precipitation energies on NO_x generation during geomagnetic storms. *Journal of Atmospheric and Solar-Terrestrial Physics*, *71*, 1176–1189. <https://doi.org/10.1016/j.jastp.2008.07.005>
- Van den Berg, J. (1999). *Wavelets in physics*. Cambridge: Cambridge University Press. <https://doi.org/10.1017/CBO9780511613265>
- Wait, J. R., & Spies, K. P. (1964). Characteristics of the Earth-ionosphere waveguide for VLF radio waves. Volume NBS Technical Note 300 NIST Research Library.
- Waters, J. W., Froidavaux, L., Harwood, R. S., Jarnot, R. F., Pickett, H. M., Read, W. G., et al. (2006). The Earth observing system microwave limb sounder (EOS MLS) on the aura satellite. *IEEE Transactions on Geoscience and Remote Sensing*, *44*(5), 1075–1092. <https://doi.org/10.1109/TGRS.2006.873771>
- Watt, A. D. (1967). *VLF radio engineering*. London: Pergamon Press.
- Zhao, H., & Zong, Q.-G. (2012). Seasonal and diurnal variation of geomagnetic activity: Russell-McPherron effect during different IMF polarity and/or extreme solar wind conditions. *Journal of Geophysical Research*, *117*, A11222. <https://doi.org/10.1029/2012JA017845>
- Zieger, B., & Mursula, K. (1998). Annual variation in near-Earth solar wind speed: Evidence for persistent north-south asymmetry related to solar magnetic polarity. *Geophysical Research Letters*, *25*, 841–844. <https://doi.org/10.1029/98GL50414>